Overactivation of a sleep-active neuron decouples survival from the need to sleep

Inka Busack[1], Henrik Bringmann[1]*

1 BIOTEC, Technical University Dresden, Germany

*Corresponding author: henrik.bringmann@tu-dresden.de

Abstract

Sleep is a state of behavioral quiescence that is closely associated with survival. Sleep-active neurons promote sleep and survival. It is not known, however, whether sleep-active neurons need to cause sleep to promote survival. Here, we tested how depolarization of the sleep-active RIS neuron in *Caenorhabditis elegans* controls sleep and survival during larval starvation. Survival always increased with raised RIS depolarization. RIS depolarization promoted sleep over a long range. Unexpectedly, however, high levels of RIS depolarization caused a nearly complete loss of sleep. Similarly, overexpression of sleep-inducing FLP-11 neuropeptides in RIS inhibited sleep, indicating that overactive transmission from RIS inhibits sleep. Despite the loss of sleep, survival was normal following FLP-11 overexpression. Thus, RIS overactivation abolishes sleep yet supports survival. These results indicate that regulation of sleep and survival are separable functions of a sleep-active neuron that are normally coupled but can be uncoupled by sleep-neuron over activation.

Author Summary

Sleep behavior and survival benefits are independently regulated functions of the sleep neuron RIS in *Caenorhabditis elegans.*

Introduction

Sleep is defined by behavioral inactivity and reduced responsiveness [1]. It is a physiological state that conserves and allocates energy, promotes restorative processes, and is important for brain and cognitive functions [2-4]. Sleep disorders and deviations from the normal sleep amount are widespread in modern societies and pose an unresolved medical and economical problem [5-7].

Central to the induction of sleep in all species are so-called sleep-active neurons that depolarize to inhibit wakefulness behavioral circuits and thus cause sleep [8, 9]. Sleep-active neurons are also important for survival, for example during starvation or after wounding [10, 11]. Little is known about how sleep-active neurons promote survival. Different hypotheses are conceivable. For example, sleep-active neurons might promote survival by reducing behavioral activities during sleep, thus conserving and allocating energy or optimizing behavior [12, 13]. The close association of sleep and physiological benefits has suggested a causal relationship. For example, memory and information processing are thought to be improved in the human brain during sleep when information inputs are blocked [14, 15], and energy is conserved by reduced behavioral activity [12]. A less explored additional hypothesis is that sleep-active neurons provide benefits during sleep, but independently of sleep behavior. According to this hypothesis, sleep-active neurons have two parallel functions. The first is to induce sleep, and the second is to promote survival. This hypothesis implies that physiological benefits of sleep-active neuron functions can be exerted also in the absence of sleep, providing a novel potential starting point for treating health problems associated with sleep loss.

Sleep is found in most animals ranging from cnidarians to humans. *C. elegans* has a small and invariant nervous system and sleep is controlled by relatively few neurons. RIS is a GABAergic and peptidergic interneuron that activates during sleep, and its ablation virtually abolishes sleep behavior [16-19]. Optogenetic manipulations showed that acute depolarization of RIS inhibits wakefulness activity such as feeding and locomotion [16, 19], whereas hyperpolarization inhibits sleep and shortens survival [10, 20-22]. RIS is

required for sleep during various stages and conditions [10, 11, 16, 17, 19, 23-27]. Larval starvation increases RIS activity and RIS is essential for starvation survival as it counteracts aging phenotype progression [10]. RIS promotes survival by controlling the transcriptional response that underlies the arrest, and promotes the activity of the FOXO transcription factor DAF-16, which is required for survival (our unpublished data) [28, 29]. Thus, RIS is a sleep-active neuron that is crucial for *C. elegans* sleep and survival.

In order to find out how RIS links sleep and survival, we determined the dose-response relationship of RIS polarization, sleep and survival. Surprisingly, we found that RIS can promote survival independently of sleep, indicating that promotion of sleep and survival are separable functions of RIS that are normally coupled during sleep. Uncoupling of the two processes provides a strategy to promote survival while gaining waking time.

Results

Generation of a strain set for controlling RIS depolarization levels

Sleep can be controlled by steering the activity of sleep-active neurons [30, 31]. We set out to control RIS activity to control sleep and survival during L1 arrest. We manipulated RIS to generate a quantitative dose-response relationship between the polarization state of RIS and sleep. For this analysis, we generated strains that express constitutively active ion channels of different strength and permeability in RIS.

To constitutively depolarize RIS, we expressed a K2P channel mutant that is permeable to sodium (*unc-58(L428F),* Fig S1A) [32] (Thomas Boulin, personal communication) tagged with mKate2 at either a lower or a higher level in RIS. The different expression levels were achieved by generating two different expression loci for the channel in the genome. To achieve a strong expression of the *unc-58(L428F)* channel (*RIS::unc-58gf(strong)*), we turned the endogenous *flp-11* locus into an operon that expressed both *flp-11* and the channel. To achieve a weaker expression of the channel (*RIS::unc-58gf(weak)*), we expressed mKate2-tagged *unc-58(L428F)* from a single-copy knock-in locus on

91 chromosome III [33], which contained only a minimal *flp-11* promoter and 3' UTR (Fig 1
92 A-D). Fluorescent imaging after two days of L1 arrest showed that the stronger strain
93 expressed at about double the level of the weaker strain and in both genetic systems, the
94 channel was expressed prominently in RIS and was targeted to the cell membrane (Fig 1A-
95 D, S1). Even after 21 days of arrest, mKate2-tagged *unc-58(L428F)* expression could be
96 detected in the strong strain indicating that RIS as well as the sodium channel are intact
97 across the entire arrest (FigS1E).
98
99 To constitutively hyperpolarize RIS, we expressed potassium channels that carry mutations
100 that cause potassium leak currents. We used different channel genes and mutations to
101 achieve different strengths of hyperpolarization (*RIS::egl-23gf(weak)* expresses *egl-*
102 *23(L229N)* in RIS, *RIS::egl-23gf(strong)* expresses *egl-23(A383V)* in RIS, and *RIS::twk-*
103 *18gf* expresses *twk-18(e1913)* in RIS) [32]. In all three strains, the channel genes were
104 knocked into the endogenous *flp-11* locus behind the *flp-11* gene to generate operons as
105 above. All protein fusions localized to the cell membrane of the sleep neuron RIS (Fig 1E-
106 H).
107
108 We measured RIS depolarization activity using calcium imaging as a proxy in these
109 transgenic strains [16]. We were able to measure RIS activity up until the first 12 days of
110 starvation and found that the effects of the channel transgenes were consistent across the
111 entire time of starvation that we analyzed (Fig. 1I for two-day starvation, S2C for all time
112 points). The mean RIS baseline calcium activity levels were reduced by the strong
113 hyperpolarization transgenes *twk-18gf* and *egl-23gf(strong)*. Depolarization levels were
114 modestly increased in *unc-58gf(weak)* and strongly increased by the *unc-58gf(strong)*
115 transgenes. The magnitude of the baseline calcium signal alterations of the different
116 transgenes were thus in accordance with the expression levels and the expected strengths
117 of the leak currents (Fig 1I). Hence, we created a set of strains that allows probing dose-
118 response relationships of depolarization levels and survival as well as sleep.
119
120 **Survival is a function of RIS depolarization**
121

122 RIS impairment has been shown to blunt survival during larval arrest and wounding [10,
123 11, 31]. We thus investigated how RIS depolarization levels affect survival in arrested first-
124 stage larval worms. For this experiment, we measured survival and the ability to recover
125 and develop to the adult stage after refeeding [10, 34]. *RIS::twk-18gf* larvae, in which RIS
126 was strongly hyperpolarized, showed strongly reduced survival by about half compared to
127 the wild type. This result is in accordance with previous reports that showed that RIS
128 ablation shortens L1 arrest survival by half, suggesting that strongly hyperpolarized RIS
129 causes similar effects on lifespan as RIS ablation [10]. *egl-23(strong)* resulted in a more
130 moderate yet significant lifespan reduction of approximately 21%. Weak hyperpolarization
131 by *egl-23(weak)* or depolarization by *unc-58gf(weak)* of RIS activity did not significantly
132 change survival. Strong RIS depolarization by *unc-58gf(strong)* had an increased survival
133 of around 19% compared to wild type (Fig 1J). To test whether this survival-extending
134 effect was caused by *unc-58gf* expression in RIS, we measured survival of *RIS::unc-*
135 *58gf(strong)* in the *aptf-1(-)* background, in which expression in RIS is abolished (Fig
136 S1G). In the combined *RIS::unc-58gf(strong); aptf-1(-)* strain the lifespan prolongation
137 was extremely shortened compared with wild type (FigS2D) and was similar to *aptf-1(-)*
138 [10] or *RIS::twk-18gf* (Fig1J), indicating that the lifespan extension indeed stemmed from
139 *unc-58gf* expression in RIS. Correlation analysis of survival time versus RIS baseline
140 activity showed that survival precipitates drastically with decreased RIS baseline activity,
141 yet increases only mildly with strong depolarization of RIS (Fig 1K). The recovery on food
142 matched the survival curves (Fig S2E). These results indicate that survival is a function of
143 RIS depolarization. The more RIS is depolarized, the more it promotes survival.
144
145 **RIS depolarization promotes survival independently of sleep behavior**
146
147 We next tracked mobility quiescence behavior to estimate sleep during L1 arrest and
148 quantified RIS activation transients [16]. Consistent with previous reports [10, 16, 18],
149 wild-type RIS showed activation transients over a constant activity baseline, and calcium
150 transients were accompanied by phases of behavioral quiescence (Fig 2A-G). Calcium
151 transients were completely abolished in both the strongest hyperpolarization strains (Fig
152 2A, B) as well as in the strong depolarization strain (2F). In the mild hyperpolarization

153 (Fig. 2C) or depolarization strains (Fig. 2E), calcium transients were still visible and
154 correlated with behavioral quiescence, but were decreased in magnitude (Fig. 2G, S2A).
155 The results suggest that RIS activation transients are required for sleep induction and that
156 strong hyperpolarization prevents these transients. Mobility quiescence decreased with
157 hyperpolarization and was increased with modest depolarization as expected. We
158 anticipated that strong RIS depolarization would even further increase sleep. Surprisingly,
159 however, mobility quiescence was completely abolished by strong RIS depolarization in
160 most of the animals (Fig. 2H). These findings were additionally confirmed for a longer
161 period of starvation up to day 12 (S2F). The loss of quiescence of the strong RIS
162 depolarization strain was similar to, but not as strong as in *aptf-1(-)* (Fig. S2G). Mobility
163 quiescence can thus be described as a parabolic function of RIS baseline calcium activity,
164 with the wild type located in the rising flank of the parabolic curve. This indicates that
165 there is a sensitive regulation of RIS-dependent sleep by modulation of RIS excitability
166 (Fig. 2I). This parabolic relationship also suggests that there is an upper limit for RIS-
167 induced sleep that might be near 50% of the time, which is consistent with the observation
168 that RIS-dependent sleep typically occurs as bouts of quiescence that are regularly
169 intermitted by bouts of wakefulness activity [10, 20, 35]. In summary, RIS polarization
170 correlates with behavioral quiescence over a wide range of conditions, except for a very
171 high level of RIS depolarization, which causes an apparent loss of sleep. This result is
172 astonishing, as strong RIS depolarization promotes survival, which could be expected to
173 depend on increased sleep. Surprisingly, strongly depolarized RIS leads to a combination
174 of increased survival with a nearly complete loss of sleep behavior. Hence, the positive
175 correlation between sleep behavior and survival that holds true for large ranges of RIS
176 polarization inverses at high levels of RIS depolarization. These data thus indicate that RIS
177 promotes sleep behavior and survival by different, separable mechanisms.
178

179 **Constant and strong RIS depolarization prevents the shutdown of wake-active**
180 **circuits**

181

182 *C. elegans* sleep is characterized as a state of globally reduced nervous system activity [10,
183 18, 27]. To test how the RIS polarization status affects neuronal activity, we quantified

184 neuronal calcium activity in the presence of different RIS polarization levels. First, we
185 measured the overall neuronal activity by utilizing a strain that expresses GCaMP6s in all
186 neurons [36]. We measured both motion behavior and overall neuronal activity by
187 extracting the calcium activity signal of all neurons as one combined signal. As expected,
188 periods of behavioral quiescence were accompanied by strongly reduced global neuronal
189 activity (Fig 3A, B, S3A-F) [10, 18, 27]. This experimental setup allowed extracting phases
190 of neuronal inactivity as well as phases of behavioral inactivity. In all strains, neuronal
191 inactivity directly correlated with immobility, suggesting that behavioral quiescence and
192 neuronal quiescence are correlated in all strains irrespective of the level of RIS polarization
193 (Fig 3C). In addition, behavioral quiescence correlated in a parabolic manner with RIS
194 activity (Fig 3D). Thus, both behavioral inactivity and brain inactivity can serve as
195 equivalent readouts for detecting sleep in this system. Strong RIS hyperpolarization led to
196 an increased mean overall neuronal activity of 50.7% compared to wild type. Intermediate
197 strength of hyperpolarization did not affect mean overall neuronal activity. Strong RIS
198 depolarization caused a significant increase of mean overall neuronal activity of 35.7%
199 (Fig 3E). These results support the notion that worms with strongly depolarized RIS are in
200 a state of wakefulness for most of the time and cannot sleep.
201
202 To further characterize the effects of our RIS-manipulating transgenes on the neuronal
203 state, we looked at the activity of specific neurons. We focused on the RIM neurons, which
204 are second layer interneurons that integrate information from sensory and internal states to
205 control motion behaviors [37, 38]. Again, we used GCaMP imaging in microfluidic
206 chambers to correlate neuronal and behavioral activity. RIM showed activation transients
207 during phases of behavioral activity. During phases of behavioral quiescence, RIM activity
208 was strongly reduced and activation transients were lacking (Fig 3F, G, S3G-L). Similar to
209 the pan-neuronal measurements, the time fraction during which RIM was inactive
210 correlated with the fraction of motion quiescence (Fig 3H, I) and followed again a parabolic
211 distribution of RIS baseline activity (Fig 3I-J). Thus, sleep can be detected consistently in
212 the RIS polarization variants by both behavioral quiescence as well as neuronal activity
213 measurements, and strong RIS depolarization inhibits neuronal signatures that are typical
214 for sleep.

215

216 Bouts of behavioral quiescence occur during transients of RIS activation, and increasing
217 RIS activity correlates with decreasing behavioral activity [10, 16]. The lack of RIS
218 activation transients caused by the strong RIS depolarization transgene might thus cause a
219 lack of behavioral quiescence. To test whether RIS depolarization transients can be
220 triggered in the strongly RIS-depolarized transgenic strain, we stimulated RIS
221 optogenetically. Optogenetic activation of RIS in the presence of the strongly depolarized
222 RIS strain did not increase RIS activation or behavioral quiescence. This result is consistent
223 with the view that strong levels of RIS depolarization prevent activation transients and thus
224 suppress sleep bouts (Fig S3M-N). In summary, these results demonstrate that sleep
225 amount is determined by the levels of RIS depolarization with both hyperpolarization and
226 strong RIS depolarization causing sleep loss.

227

228 **Both deletion and overexpression of *flp-11* inhibit sleep behavior**

229

230 How can strong and constant RIS depolarization inhibit sleep? Constant RIS depolarization
231 might cause an increased secretion of neurotransmitters from RIS, which in turn could lead
232 to desensitization or habituation effects of the sleep-inducing system, ultimately leading to
233 reduced sleep. FLP-11 is a neuropeptide of RIS that contributes to sleep induction [17].
234 Expression from the *flp-11* promoter depends on neuronal activity levels [39], and is
235 increased in *RIS::unc-58gf(strong)* (Fig S2B). To directly test the role of FLP-11 in
236 quiescence during L1 arrest, we measured the effects of overexpressing *flp-11* in RIS (*flp-*
237 *11OE*) by using a multicopy transgenic extrachromosomal array that expresses FLP-11
238 from its own promoter, and compared the effects of *flp-11OE* with the effects of *flp-11*
239 deletion (*flp-11(-)*) (Fig S4A-B) [17]. Both *flp-11OE* and *flp-11(-)* strongly reduced
240 quiescence behavior, and where thus similar to *RIS::unc-58gf(strong)* (Fig 4A). *RIS::unc-*
241 *58gf(strong)* still displayed a small fraction of quiescence behavior during L1 arrest. To
242 test whether this residual quiescence was caused by *flp-11*, we combined *RIS::unc-*
243 *58gf(strong)* with either *flp-11(-)* or *flp-11OE,* and quantified quiescence behavior. For this
244 experiment, we deleted the entire *flp-11* gene in the *RIS::unc-58gf(strong)* operon locus.
245 The sleep loss of *RIS::unc-58gf(strong)* was reduced further by both *flp-11(-)* and also by

246 *flp-11OE,* suggesting that the residual quiescence behavior in *RIS::unc-58gf* indeed
247 depends on *flp-11* (Fig 4A).
248
249 How does *flp-11OE* affect RIS activity? To answer this question, we first investigated
250 calcium activity of RIS in *flp-11OE* animals. RIS calcium activity stayed at a constant level
251 and did not show any activation transients in most of the animals that were tested (Fig 4B-
252 D). We next tested whether RIS can be optogenetically excited in *flp-11OE*. Unlike in wild-
253 type animals, optogenetic activation of RIS in *flp-11OE* animals did not increase calcium
254 activity (Fig 4E). In summary these experiments indicate that excess FLP-11 inhibits the
255 activation dynamics of RIS and the behavioral quiescence of sleep, suggesting that similar
256 effects might underly inhibition of sleep in *RIS::unc-58gf(strong)*.
257
258
259 **FLP-11 neuropeptides support survival**
260
261 *flp-11* is required for most of the sleep during L1 arrest. We hence tested whether FLP-11
262 neuropeptides are also required for survival. Deletion of *flp-11* reduced survival by 24.7%,
263 suggesting that *flp-11* contributes to survival (Fig. 4F). To test whether *flp-11* is required
264 for increased survival caused by *RIS::unc-58gf(strong)*, we measured survival in the
265 *RIS::unc-58gf(strong), flp-11(-)* strain. *flp-11(-)* suppressed almost the entire survival
266 extension caused by *RIS::unc-58gf(strong)* (Fig. 4F). We next tested the effects of *flp-*
267 *11OE* on survival. *flp-11OE* did not significantly change survival, and it efficiently
268 suppressed the extended survival of *RIS::unc-58gf(strong)* (Fig. 4G). Consistent with the
269 survival assays, the recovery of larvae from the arrested first larval stage was significantly
270 reduced by *flp-11(-)*, yet unaffected by *flp-11OE* (Fig S4C-D). Together these experiments
271 indicate that *flp-11* plays an important role in survival and recovery of L1 arrest both in the
272 wild type and in *RIS::unc-58gf(strong)*.
273
274 These results suggest that *flp-11* plays two roles, one role is to promote sleep and the other
275 is to promote survival. *flp-11OE* uncouples those two functions of *flp-11*. Hence, *flp-11OE*
276 presents a condition in which, similar to *RIS::unc-58gf(strong)*, the animals survive well

277 without much sleep. Deletion of *flp-11* blunts survival less than strong RIS
278 hyperpolarization, suggesting that additional neurosecretory factors might also contribute
279 to survival. As RIS expresses multiple neuropeptides and also GABA [17, 19, 23], it may
280 use multiple transmitters to control survival. In summary these data suggest that FLP-11
281 neuropeptides are the major transmitters released by RIS to promote both sleep as well as
282 survival during L1 arrest.
283
284 **Discussion**
285
286 Sleep-active neurons inhibit wakefulness to cause sleep and promote survival [30, 31]. A
287 parsimonious explanation linking these two observations would be that sleep promotes
288 survival, for example through energy conservation or behavioral optimization [13]. Our
289 data, however, suggest that the sleep-active RIS neuron promotes survival rather
290 independently of sleep. This suggests that RIS has two parallel functions. The first function
291 is the induction of sleep, a state of reduced nervous system activity and behavioral
292 quiescence. The reduction of brain and muscle activity likely contributes to survival by
293 conserving energy. While energy consumption appears to be playing a role in survival,
294 behavioral activity and thus energy consumption does not correlate with survival when
295 transmission from RIS is strongly increased. In strongly depolarized *RIS::unc-58gf(strong)*
296 animals, neuronal and behavioral activity are high and consume energy, yet survival is
297 increased. Similarly, in *flp-11OE*, behavioral activity is as high as in RIS loss-of-function
298 mutations, which should cause high energy expenditure, yet the survival is normal. Hence
299 RIS appears to be able to promote survival rather independently of sleep behavior and
300 associated energy conservation. As both sleep and survival are functions of RIS
301 depolarization over a wide range of conditions, the two processes are normally coupled
302 during sleep. During each sleep bout, RIS depolarizes and thus promotes both sleep as well
303 as survival. This coupling of sleep and survival processes might ensure that phases of brain
304 and behavioral inactivity coincide with phases during which survival-promoting processes
305 are active. This tight coupling might serve to optimize energy expenditure, as energy
306 conserved by sleep could be directly allocated to survival-promoting processes [12].
307

308 Both, the induction of sleep and the promotion of survival by RIS depend on FLP-11
309 neuropeptides, which are released upon depolarization. Hence the role of FLP-11 on
310 survival could include the conservation of energy during sleep plus an additional survival
311 component that is independent of sleep. The effects of FLP-11 on sleep and survival can
312 be separated by their different response to increased FLP-11 activity. The two functions of
313 FLP-11 might separate mechanistically at the level of divergent receptors, signaling
314 pathways or cell types downstream of FLP-11 that mediate either the sleep or the survival
315 response.
316
317 By controlling the polarization state of RIS, we showed that the survival function and the
318 sleep function of this sleep neuron can be decoupled. By strongly depolarizing RIS, we
319 generated a condition in which wakefulness neural activity and sleep-active neuron
320 depolarization coexist. The coupling of sleep and survival functions by sleep-active
321 neurons also could provide a starting point for treating the consequences of insomnia in
322 humans. Monitoring and managing the activity of sleep-active neurons might be key to not
323 only restore sleep but also to promote essential physiological functions.
324
325

326 **Figures**

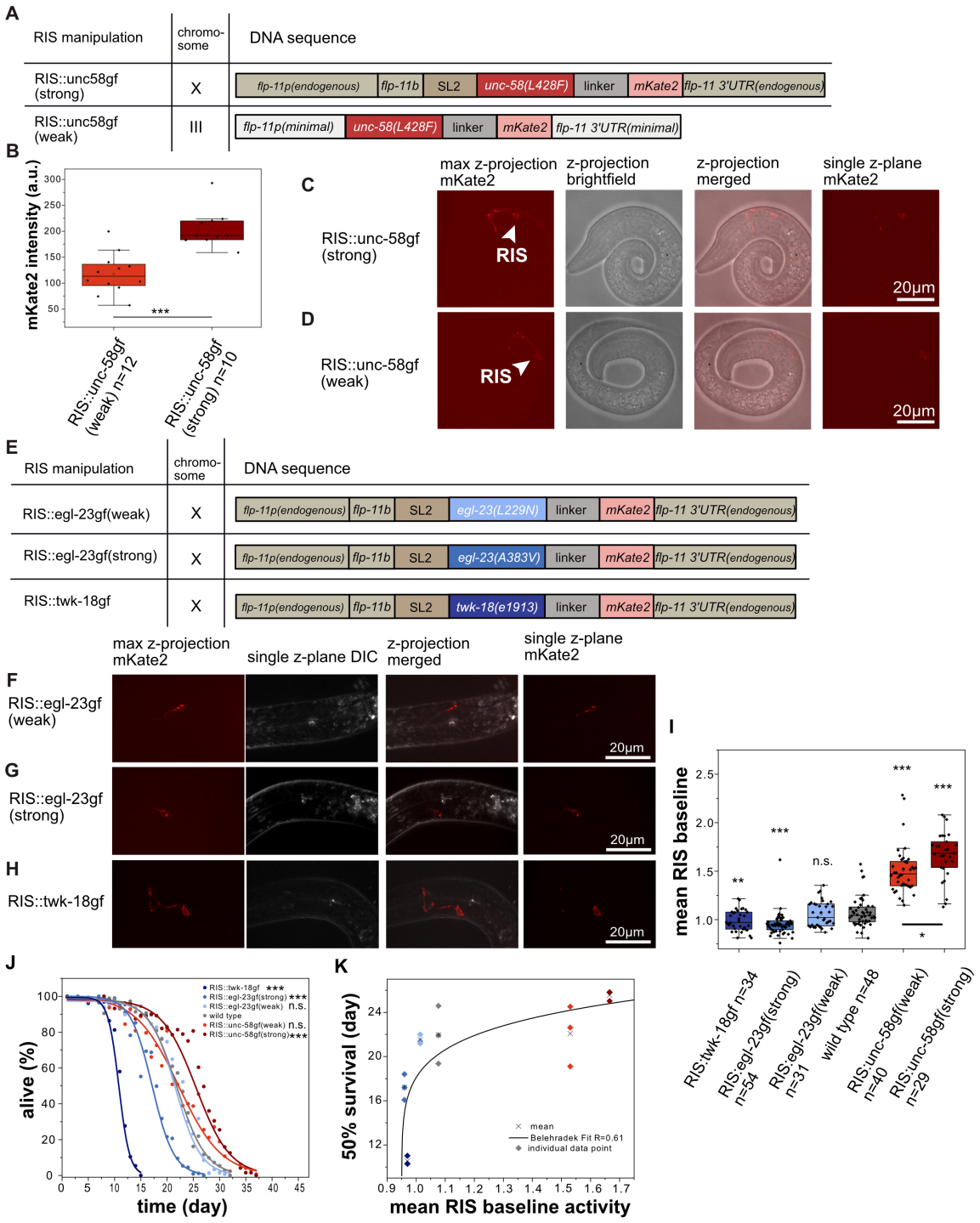

327

328 **Fig. 1 – RIS depolarization promotes survival**

329 A) Schematic representation of the genetic design of the different RIS depolarization

330 transgenes.

331 B) Quantification of the expression levels of UNC-58gf::mKate2 in the two RIS
332 depolarization strains. ***p<0.001, Welch test.
333 C) Localization and expression of the strong depolarization strain (*RIS::unc-*
334 *58gf(strong)*).
335 D) Localization and expression of the weak depolarization strain (*RIS::unc-58gf(weak)*).
336 E) Scheme of the genetic design of the different RIS hyperpolarization transgenes.
337 F-H) Localization and expression of mKate2, which is translationally fused to the ion
338 channels, in the different hyperpolarization strains.
339 I) Ion channel expression in RIS results in a dose-response strain set with varying levels
340 of RIS baseline activity. n.s. p>0.05, **p<0.001, ***p<0.001, Welch test with FDR
341 correction for multiple testing.
342 J) Strong hyperpolarization significantly decreases survival whereas strong depolarization
343 prolongs survival (three-parameter logistic fit, see also supplementary table S1, Fisher's
344 Exact Test was conducted when 50% of wild-type worms were alive (day 22)). The p-
345 values were FDR corrected with Benjamini-Hochberg procedure with a 5% false
346 discovery rate. The plot includes data from three replicates. ***p<0.001.
347 K) Survival time increases with mean RIS baseline activity from a minimum median of
348 about 10 days to a maximum median of about 25 days (Belehradek fit, timepoints when
349 50% of worms of a strain were still alive are plotted for all three replicates).
350

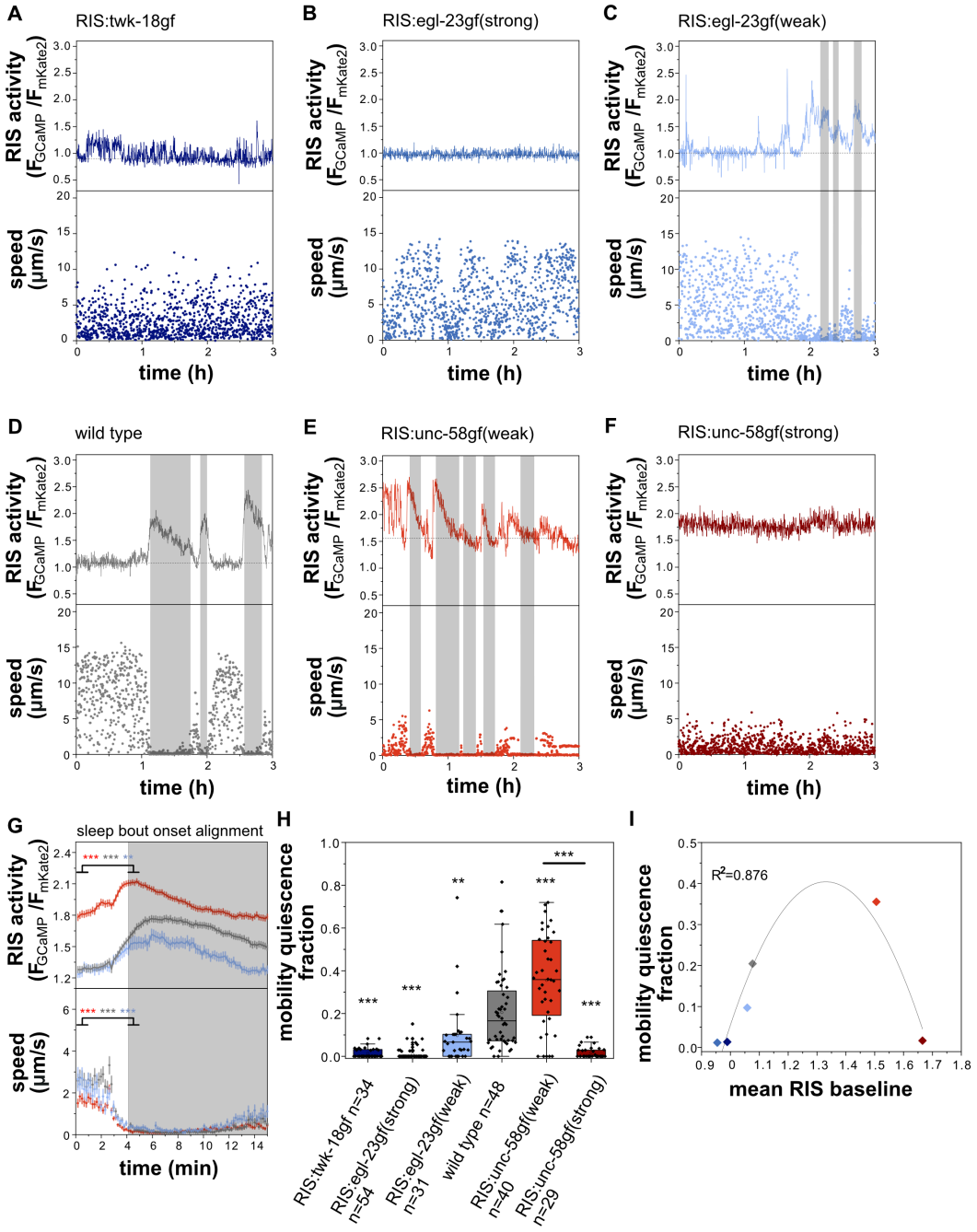

Fig. 2 – Both, strong hyperpolarization as well as strong depolarization of RIS prevent sleep behavior

356 A-F) Ion channel expression in RIS controls calcium activity and sleep behavior.
357 Mobility quiescence bouts (grey shade) correlate with RIS transients A) RIS-
358 hyperpolarized strain *RIS::twk-18gf* and B) RIS-hyperpolarized strain *RIS::egl-*
359 *23gf(strong)* larvae do not have detectable mobility quiescence bouts or RIS transients.
360 C) The weakly RIS hyperpolarized strain *RIS::egl-23gf(weak)* has reduced mobility
361 quiescence bouts. D) Wild-type RIS activation transients and immobility bouts. E) The
362 weakly RIS-depolarized strain *RIS::unc-58gf(weak)* spends more time in mobility
363 quiescence bouts. F) The strongly RIS depolarized strain *RIS::unc-58gf(strong)* has no
364 detectable mobility quiescence bouts and no RIS transients but a high constant activity.
365 G) RIS activation and immobility are correlated. Alignment of RIS activity and speed to
366 mobility quiescence bout onset. **$p<0.01$, ***$p<0.001$, Wilcoxon signed rank test.
367 H-I) Both, strong hyperpolarization as well as strong depolarization of RIS prevent sleep
368 behavior. I) mobility quiescence is a function of RIS activity levels n.s. $p>0.05$,
369 **$p<0.001$, ***$p<0.001$, Welch test with FDR correction for multiple testing. J) second-
370 degree polynomial fit for mobility quiescence fraction against mean RIS baseline activity.
371 Most of the channel transgenes are expressed as an operon with *flp-11*, which should not
372 grossly impair expression of the *flp-11* neuropeptide gene that is crucial for quiescence
373 induction [17, 19]. The correlation of quiescence with RIS polarization levels and the
374 preservation of most sleep bouts in the weak *egl-23* knock-in transgene support this
375 notion.
376

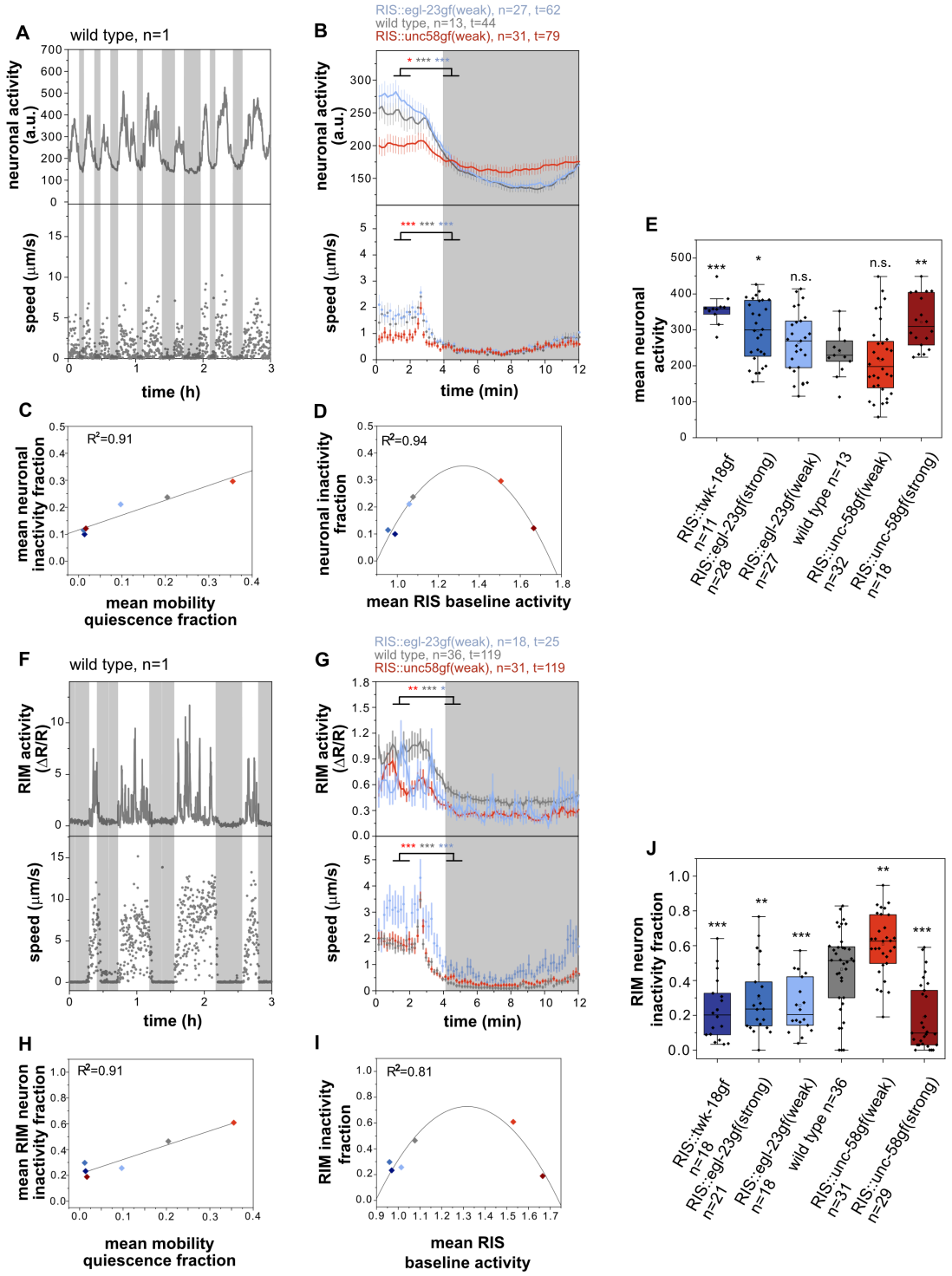

Fig. 3 – Constant strong RIS depolarization fails to inhibit wake-active circuits

A-B) Reduced global neuronal activity (grey shading) correlates with motion quiescence (supplementary movies S1-S6). A) sample trace, B) alignment of overall neuronal activity to mobility quiescence bout onset. ***p<0.001, Wilcoxon signed rank test.

382 C) The mean neuronal inactivity fraction correlates with the mean mobility quiescence
383 fraction (linear fit) for all strains.
384 D) Both, strongly hyperpolarized as well as strongly depolarized strains spend only a
385 small fraction of time in states of neuronal inactivity (parabolic fit).
386 E) Strong RIS hyper- as well as depolarization caused an overall increase of neuronal
387 activity. n.s. $p > 0.05$, *$p<0.05$, **$p<0.01$, ***$p < 0.001$, Welch test with FDR correction
388 for multiple testing.
389 F-G) RIM does not activate during mobility quiescence bouts. F) sample trace (grey
390 shade is RIM inactivity bout). G) Alignment of RIM activity and speed to mobility
391 quiescence bout onset. *$p<0.05$, **$p<0.01$, ***$p<0.001$, Wilcoxon signed rank test.
392 H) The mean RIM inactivity fraction correlates with the mean mobility quiescence
393 fraction (linear fit) for all strains.
394 I) Both, strongly hyperpolarized as well as strongly depolarized strains spend only a
395 small fraction of time in states of RIM inactivity (parabolic fit).
396 J) Strong RIS hyper- as well as depolarization caused an overall increase of RIM activity.
397 **$p < 0.01$, ***$p < 0.001$, Welch test with FDR correction for multiple testing.
398

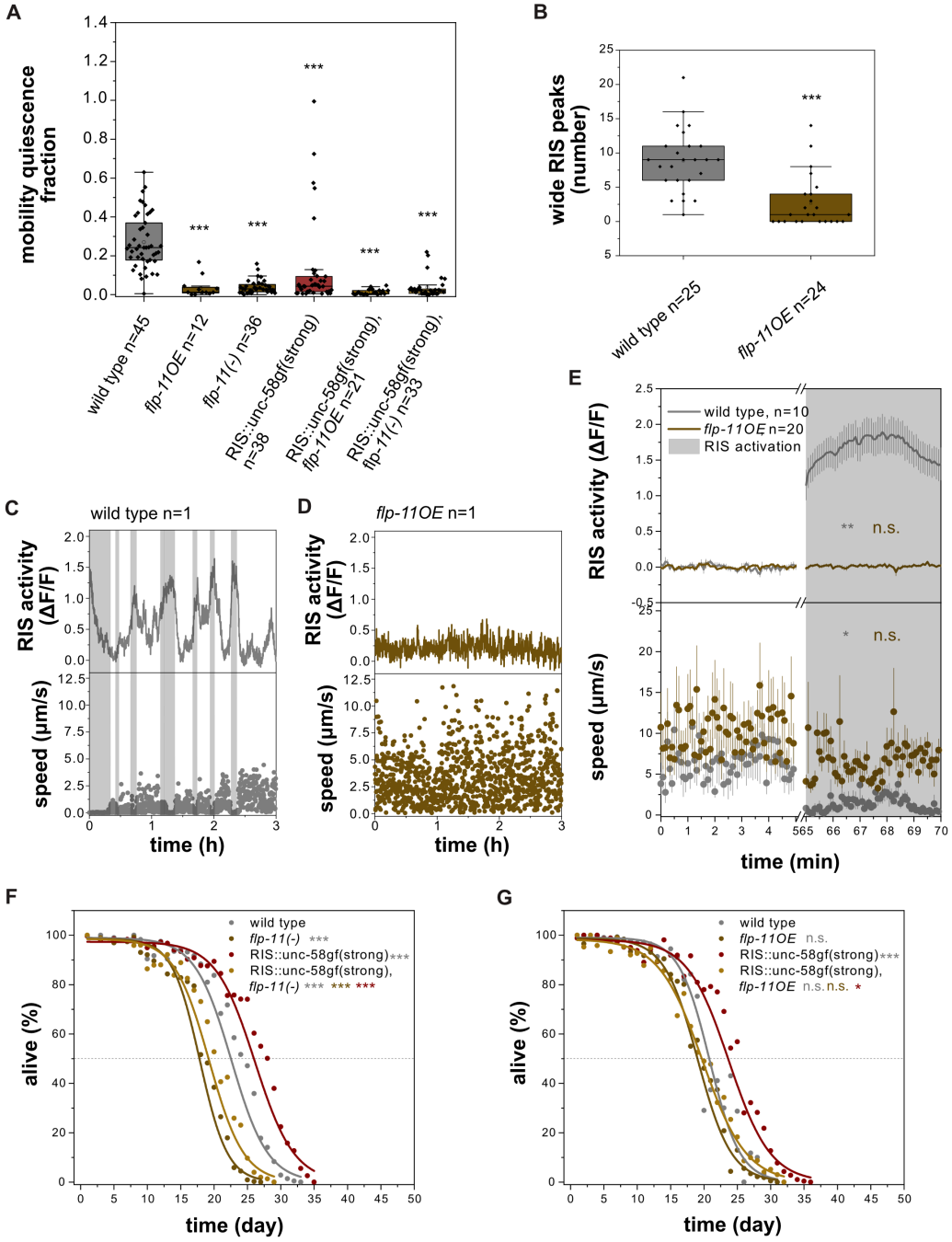

Fig 4 – FLP-11 controls sleep and survival during L1 arrest

A) Deletion as well as overexpression of the neuropeptide gene *flp-11* causes loss of sleep. The strongly RIS depolarized worms (*RIS::unc-58gf(strong)*) sleep even less when

403 *flp-11* is deleted or overexpressed. ***p<0.001, Welch test with FDR correction for
404 multiple testing.
405 B) Sample trace of RIS activity and speed of a wild type worm.
406 C) Sample trace of RIS activity and speed of a worm overexpressing *flp-11*.
407 D) *flp-11OE* worms do not show many RIS peaks. ***p<0.001, Welch test.
408 E) Optogenetic activation of RIS causes a strong RIS activity increase and reduction of
409 speed in the wild type, but there is no response in the *flp-11OE* strain. n.s. p>0.05,
410 ***p<0.001, Wilcoxon signed rank test.
411 F) Loss of the neuropeptide FLP-11 leads to strongly reduced survival (three-parameter
412 logistic fit, see also supplementary table S1, Fisher's Exact Test was conducted on day
413 18) for comparisons when *flp-11(-)* was the shortest lived condition, day 20) when
414 *RIS::unc-58gf(strong), flp-11(-)* was the shortest lived condition or day 24) when wild
415 type was the shortest lived condition. The p-values were FDR corrected with Benjamini-
416 Hochberg procedure with a 5% false discovery rate. The plot includes data from three
417 replicates. ***p<0.001.
418 G) Overexpression of FLP-11 does not reduce survival (three-parameter logistic fit, see
419 also supplementary table S1. Fisher's Exact Test was conducted on day 23). The p-values
420 were FDR corrected with Benjamini-Hochberg procedure with a 5% false discovery rate.
421 The plot includes data from three replicates. *p<0.05, ***p<0.001.
422
423 **Materials and Methods**
424
425 **Resource and Materials Availability**
426 Key *C. elegans* lines that were used in this project are available at the Caenorhabditis
427 elegans Genetics Center. Other *C. elegans* strains, plasmids, or additional reagents
428 generated for this study are available upon reasonable request.
429
430 **Data and Code Availability**
431 Raw and processed data as well as MATLAB scripts will be made publicly available.
432
433 **Experimental model and subject details**

434 *C. elegans* hermaphrodites were maintained at 20°C. They were kept on Nematode Growth
435 Medium Plates (NGM). The *Escherichia coli* strain OP50 served as a food source during
436 maintenance [40].
437
438 **Method Details**
439
440 **Creation of transgenic animals**
441
442 **Crossing *C. elegans* strains**
443 Males were generated via heat shock or maintained by a continuation of crossings of
444 worms of the same genotype [41]. Single worms of the F2 generation were genotyped
445 using duplex PCR genotyping [42]. For crossing fluorescent transgenes, fluorescent
446 markers were used. All strains and primers of this study can be found in the
447 supplementary tables S2 and S3.
448
449 **Creating mutants with the CRISPR/Cas9 system**
450 We designed the sequences of the following transgenes in silico. Transgenes were
451 synthesized and inserted into the genome by using CRISPR/Cas9 by SunyBiotech.
452 Transgene sequences were verified through Sanger sequencing.

453

454 PHX1433 *flp-11(syb1433 [flp-11-SL2-egl-23cDNA(A383V)-linker-mKate2]) X*
455 PHX1445 *aptf-1(gk794) II; flp-11(syb1445[flp-11-SL2-unc-58(L428F)-linker-*
456 *mKate2]) X*
457 PHX1464 *flp-11(syb1464[flp-11-SL2-egl-23cDNA(L229N)-linker-mKate2]) X*
458 PHX2193 *flp-11(syb2193[flp-11b-SL2(gpd-2)-mKate2-linker-twk-18(e1913)]) X*
459 PHX2493 *lgc-38(syb2346[flp-11p::dpy-10 site::flp-11 3'UTR], syb2493[ReaChR-*
460 *linker*-mKate2]) III.
461 PHX3190 *lgc-38(syb2346[flp-11p::dpy-10 site::flp-11 3'UTR] ,syb3190[unc-*
462 *58(e665)-linker(GSGSGSGSG)-mKate2]) III*

463 PHX4110 *lgc-38(syb2346[flp-11p::dpy-10 site::flp-11 3'UTR], syb4110[unc-58gf-*
464 *CAI-1.0-linker(GSGSGSGSG)-mKate2]) III*
465 PHX4416 *aptf-1(gk794) II; flp-11(syb1445 syb4416) X*
466

467 The coding sequences of the ion channel transgenes were synthesized and consisted each
468 of the spliced coding sequence of the ion channel including the mutation that caused the
469 leak current [32], a C-terminal linker sequence followed by a C-terminal mKate2 gene.
470 The coding sequence of mKate2 was codon optimized and intronized [43]. The coding
471 sequences of the ion channels were not codon optimized to allow for proper folding of
472 the membrane proteins. We tried codon-optimization [43] of the *unc-58(L428F)* channel
473 gene and mKate2 to achieve high expression, but this also caused aggregation of the
474 fluorescent fusion protein (Fig S1A,D). Hence, we used the endogenous gene sequence
475 for the channel and only codon-optimized mKate2.

476 Analysis of the RIS transcriptome showed that *flp-11* has the strongest and most specific
477 promoter of all RIS-expressed genes, with 157-fold higher expression in RIS than in other
478 neurons [23]. *flp-11* is also expressed in other neurons, albeit at low levels [17, 23, 44].
479 Using imaging settings that cause oversaturation of the mKate2 signal in RIS revealed that
480 there is a weak expression of *unc-58gf::mKate2* in a few neurons in the ventral cord in
481 *RIS::unc-58gf(strong)* (Fig S1F). Expression from the *flp-11* promoter in RIS but not in
482 other neurons depends on APTF-1 [17]. We hence imaged mKate2 expression in *aptf-1(-*
483 *)*. Consistent with previous results [17], mKate2 expression was abolished in RIS but was
484 still present in the ventral cord (Fig S1G). Thus, expression from the *flp-11* promoter is
485 strong, has a high level of RIS specificity, and RIS expression depends on *aptf-1*.
486

487 The sequences of the ion channels of the strains PHX1433, PHX1445, PHX1464 and
488 PHX2193 were inserted after the stop codon of the *flp-11* endogenous coding sequence
489 together with an SL2 site. Thus, an operon was created that expressed both *flp-11* and the ion
490 channel gene from the *flp-11* promoter. The transgenes of PHX2493, PHX3190 and
491 PHX4110 were generated via a single-copy knock-in loci for defined gene expression (SKI
492 LODGE) system [33]. For the SKI LODGE expression in RIS we first inserted the minimal

493 *flp-11* 3' and 5'UTRs separated by a *dpy-10* sgRNA cutting site. The expression from these
494 minimal UTR sequences allowed specific expression in RIS, but the expression levels were
495 lower compared with the endogenous *flp-11* locus (Fig 1A-D, S1A-D). The final sequences
496 of all transgenes can be found in the supplementary Text S1.

497

498 # Imaging

499

500 **Microfluidic devices**

501

502 Worms were filmed in microfluidic devices made from agarose hydrogel as previously
503 described [45, 46]. In brief, a PDMS mold was used to cast box-shaped indentations from
504 melted 5% agarose diluted in M9 buffer. After agarose hydrogel solidification the stamp was
505 removed resulting in hundreds of microchambers sized 110x110x10µm per agarose slab.
506 Depending on the experiment, approximately 9-20 pretzel-stage eggs per strain were then
507 transferred without food into the indentations in the hydrogel and the chambers were closed
508 with a coverslip and kept in a temperature-controlled dish. Hatching of the larvae in the absence
509 of food caused L1 arrest. Chambers were timed so that the worms were incubated for 48h at
510 25°C before imaging. The number of biological replicates (n) imaged in microfluidic devices
511 is stated in each figure. There were two or more technical replicates (different microfluidic
512 devices) imaged for each experiment.

513

514 **Software**

515

516 All image acquisition was performed with Nikon NIS Elements 5 software (Nikon, Tokyo).

517

518 **Dark Differential Contrast (DIC) Imaging**

519 Long term dark differential contrast (DIC) images were acquired with a standard 100W
520 halogen lamp and an infrared filter (Semrock Brightline HC 785/62) (Idex Health and Science,
521 New York). The images were taken 48h upon starvation for 12h with a frame rate of 0.1Hz.
522 A 20x objective for imaging was combined with a 0.7 lens.

523

524 **Functional Ca^{2+}-imaging**

525 For calcium imaging we used either a back-illuminated sCMOS camera (Photometrics Prime
526 95B, 1200x1200 pixels) (Figure 1I, 2, S2A-C) or an Andor iXon EMCCD camera (512x512
527 pixels, Andor Technology Ltd., Belfast). (Figure 3, 4B-D, S3A-L). The gain of the iXon
528 camera was set to 200. The iXon camera's read out mode was 10MHz at 14-bit. The images
529 of the Photometrics camera were 2 x 2 binned.
530
531 A 20x objective was used to simultaneously image 3 x 3 adjacent microchambers containing
532 one worm each (This configuration was used to obtain data for Figures 3, 4B-D, S3A-L). A
533 10x objective combined with a 1.5x lens was used to simultaneously image 6 x 6 adjacent
534 microchambers containing one worm each (this configuration was used to obtain data for
535 Figures 1I, 2, S2A-C).
536
537 For calcium imaging we utilized a 480nm LED and a standard GFP filter set (EGFP,
538 Chroma). The EMCCD camera TTL signal triggered the LED. For data in Figures 1I, 2 and
539 S2A-B the 490nm intensities were set to either 0.23mW/mm^2 with an exposure time of 50ms
540 (Figure 1I, 2, S2A-B), 0.33mW/mm^2 (Figure 3A) or 0.51 mW/mm^2 (Figure 3B), both with an
541 exposure time of 5ms. Additional mKate2 fluorescence images were acquired for the RIS and
542 RIM activity experiments (Figure 1I, 2, 3B S2A, S3G-L). For this measurement we used a
543 585nm LED and a set of standard Texas Red filters (Chroma). The 585nm LED intensity was
544 set to 0.11mW/mm^2 while imaging with a 50ms exposure time (Figure 1I, 2, S2A, B) and to
545 0.15 mW/mm^2 for acquiring images with a 100ms exposure time (Figure 3F-J). Calcium and
546 mKate2 imaging were carried out with a frame rate of 0.1Hz for 3h. As the ion channels were
547 additionally tagged with an mKate2, the parental strains without the GCaMP/mKate2
548 construct were imaged with the same settings with the 585nm LED. Here, no signal could be
549 observed in the parental strains.
550 For the long-term calcium imaging from day 1 to day 12 we utilized slightly different LED
551 light intensities. Here, the 490nm intensity was set to 0.34mW/mm^2 and the 585nm light had
552 an intensity of 0.21mW/mm^2.
553 RIS in the *flp-11OE* strain could only be imaged for GCaMP as the overexpression construct
554 carried mKate2, which caused an extremely bright signal that did not allow for normalization
555 of the GCaMP signal. A 490nm light of 0.15mW/mm^2 intensity was utilized.
556

557

558 **Optogenetic activation**

559

560 For optogenetic RIS activation experiments, the agarose containing the microchambers was
561 supplemented with 10µl of 10mM all-trans-retinal (ATR, Sigma Aldrich) 1h before the start of
562 image acquisition. Control worms and worms before the stimulation did not receive ATR
563 treatment.

564

565 In experiment in Fig S3M-N, A baseline of GCaMP images was recorded for 1min with a
566 frame rate of 0.33Hz. This was followed by a stimulation phase of 1min, in which again
567 GCaMP images were acquired with a frame rate of 0.33Hz. In between the camera exposures,
568 the worms were illuminated with 585nm LED light with an intensity of 0.17mW/mm^2 for
569 800ms triggered by the software. After the stimulation period, a recovery period of 1min was
570 imaged, in which GCaMP images were acquired with a frame rate of 0.33Hz. The 490nm LED
571 intensities for imaging were set to 0.39mW/mm^2 and images were acquired with an exposure
572 time of 5ms.

573

574 In the optogenetic experiment in Fig 4E the worms were first imaged without ATR for 5min.
575 With a 490nm LED of 0.36mW/mm^2 intensity, GCaMP was imaged with a frame rate of 0.2Hz
576 and exposure time of 50ms. mKate2 images were additionally acquired with a 585nm LED
577 with an intensity of 0.25mW/mm^2 for 50ms all 5s. After the pre stimulation phase, 10µl of
578 10mM all-trans-retinal (ATR, Sigma Aldrich) was added to the worms and the imaging
579 protocol was then repeated after 1h to allow for sufficient time for the worms to ingest the
580 ATR.

581

582 **Expression of mKate2 of the RIS activity strains**

583

584 Larvae were synchronized via bleaching [23] and hatched in M9 buffer at 25°C. Imaging of
585 most strains was performed after 48h in the L1 arrest stage by transferring worms with a 10
586 µl liquid drop onto an agarose pad (5% agarose solved in M9 buffer). The *flp-11OE* and
587 *RIS::unc-58gf, flp-11(-)* worms were imaged 24h after bleaching. Larvae were then fixed
588 through the addition of 10 µl of 25mM levamisole (Sigma Aldrich).

589

590 To image the expression levels of the different RIS activity transgenes, mKate2 was imaged
591 with an Andor Revolution disc system (Andor Technology Ltd.) and a CSU-X1 spinning disc
592 head (Yokogawa). The 561nm laser light intensity was set to 0.49mW/mm^2. The worms were
593 imaged through a 100x oil objective and by an Andor iXon Ultra EMCCD camera
594 (1024x1024 pixels) (Andor Technology Ltd., Belfast). An EM gain of 200 was included and
595 the camera read-out time was set to 30MHz. A z-stack of 21planes, each 0.5µm apart (10µm
596 in total) was acquired. For comparison, a maximum z-stack projection was calculated.
597

598 ## Image analysis

599 **DIC images analysis**

600

601 Mobility of worms was analyzed from DIC images though image subtraction [47]. The matrix
602 of intensity values of the preceding image was subtracted from the matrix of intensity of the
603 following image. A mean of all values of the difference matrix was then calculated to attain a
604 mean smoothed image subtraction value, which represents the movement of the worm.
605

606 **Analyzing functional Ca^{2+}-images**

607 Neuronal intensities were automatically analyzed via custom-written MATLAB scripts.
608 These codes extracted the regions of interest through an intensity threshold and acquired
609 the intensities and position data. The extracted regions were set to be slightly bigger than
610 the actual size of the neuron to allow for background intensity detection and background
611 subtraction. The pan-neuronal activity was measured treating the head neurons as a
612 combined signal. The RIS GCaMP activity in Figure 2 was determined by extracting the
613 position data of the corresponding mKate2 signal. A larger region of interest was extracted
614 and a fitting percentage of that was calculated as the signal. The extracted position data of
615 the signal served to calculate the speed values.
616

617 RIS and RIM activities were normalized by dividing GCaMP intensities through
618 corresponding mKate2 intensities. In the optogenetic experiment, the baseline
619 measurements were used for normalization.
620

621 **Mobility quiescence detection**

622 First, speeds or image subtraction mean intensities were smoothed over 30 time points
623 through the *smooth* function in MATLAB, which is a first-degree polynomial local
624 regression model. Smoothed speeds and image subtraction values were normalized
625 between 0 and 1 for each individual animal with 0 being the lowest speed value and 1 the
626 highest speed value the animal possessed. A mobility quiescence bout was counted when
627 the normalized speed was below a specific percentage for a certain amount of time. For
628 calcium imaging experiments with the 20x objective (Figure 3), the normalized speed had
629 to be below 10% for at least 3min. The RIS activity experiment, which was filmed with a
630 10x objective, required a percentage threshold of 5% for a minimum of 4min. For DIC
631 images filmed with the 20x objective, the normalized mean image subtraction values had
632 to be below 15% for at least 3min to be counted as sleep time points.

633

634 **Mobility quiescence bout onset alignment**

635 Speeds and GCaMP intensities were aligned to the start of mobility quiescence bouts, which
636 had been detected by the mobility quiescence bout analysis. Mobility quiescence bouts were
637 only counted for the alignment when the worm was mobile throughout 3min prior to the
638 mobility quiescence bout onset. This alignment was carried out with a custom-written
639 MATLAB script.

640

641 **Neuronal inactivity detection**

642

643 The neuronal activities were treated similarly as speed values for the mobility quiescence
644 detection. However, the nervous system was counted as inactive when it was below 20%
645 of the smoothed and normalized activity for at least 3min.

646

647 **RIM neuron inactivity detection**

648 RIM peaks were detected through custom-written MATLAB scripts. First, the activity values
649 were smoothed using the inbuilt *smooth* function over 5 time points. Then, peaks of a
650 minimum prominence of 0.2 were extracted via the inbuilt function *islocalmax.* RIM was
651 counted as inactive when there were no detected peaks for at least 5min.

652

653 **Wide RIS peak extraction**

654 To quantify RIS transients, a custom-written MATLAB script was utilized. The in-build
655 function *findpeaks* detected peaks with a minimum peak width of 9 frames, which
656 corresponds to peak time of 1.5min.

657

658 ## Survival assay

659 Worms were synchronized by bleaching [23]. 3-4 days before bleaching, 10-12 L4 stage
660 worms were transferred onto NGM plates with a diameter of 6cm. 1-2 plates were bleached
661 per strain and the day of bleaching was defined as day 0. The following day was counted
662 as day 1 of the lifespan. During the survival assay, the worms were kept in liquid culture
663 in 1ml M9 buffer in 2ml Eppendorf tubes. This resulted in a population density of
664 approximately 100 worms per 10µl. The tubes were placed in a rotator at 20°C, which
665 rotated at 20rpm. For counting, 2x5µl drops of the liquid culture were pipetted onto fresh
666 NGM plates for each strain respectively. The worms were allowed to recover for at least 2h
667 after pipetting before counting. Counting was performed manually with the assistance of a
668 clicker. The recovery number, i.e., the number of worms that developed into at least the L4
669 stage, was counted 3-5 days after pipetting. Around 50-100 worms were counted for each strain
670 of each replicate on each time point except for the *flp-11OE* strains. As the *flp-11OE* strains
671 were extra chromosomal with medium transmission rate only 20-60 worms could be counted
672 for each strain on one day in each replicate.

673

674 ## Fitting

675 Origin software was used for the regression analyses. A second-degree polynomial was
676 fitted to the data in Figure 2I, 3D and 3I. A linear regression was fitted to the data in Figure
677 3C and 3H. For data in Figure 1K a Belehradek fit was conducted. R^2 values can be found
678 in the corresponding figures. The exact functions are in Table 1.

679

Figure panel	fit	function
1K	Belehradek fit	$y = 28.693 * (x - 0.97774)^{0.14966}$
2I	2nd degree polynomial	$y = -5.7210 + 9.2995x - 3.5059x^2$
3C	linear	$y = 0.116 + 0.5494x$

3D	2nd degree polynomial	$y = -3.067 + 5.163x - 1.95x^2$
3H	linear	$y = 0.21203 + 1.10949x$
3I	2nd degree polynomial	$y = -6.38841 + 10.8x - 4.1x^2$

Table 1. Calculated functions for the regressions.

Quantification and Statistical Analysis

The experimenter was blind to the genotype information during the lifespan experiments. All other experiments relied on an automated analysis and hence were not blinded. The Wilcoxon signed rank test was utilized for the comparison of speeds and GCaMP intensities within the same strain. The Welch test was conducted to compare data from different strains. The survival assay experiments were statistically analyzed by utilizing the Fisher's exact test at 50% survival of the wild type. Experiments with four or more genotypes were FDR corrected by the Benjamini-Hochberg procedure with a 5% false discovery rate. The graphs depict the mean and standard error of the mean. Box plots display individual data points, the interquartile range and the median. The whiskers represent the 10-90th percentile.

Acknowledgements

We thank the *Caenorhabditis* Genetics Center supported by the National Institutes of Health Office of Research Infrastructure Programs (P40 OD010440) for strains. The CRISPR strains were generated by SunyBiotech based on our design. We thank Thomas Boulin for communicating the sodium permeability of *unc-58gf* and suggesting its use as a tool for neuronal depolarization. This work was supported by a European Research Council Starting Grant (ID: 637860, SLEEPCONTROL).

Author contributions

I.B. designed, executed and analyzed all experiments. H.B. conceived the overall structure of the study, designed the transgenes, acquired funding and supervised the project. All authors wrote the paper.

Declaration of Interest

The authors declare no competing interests.

708 **References**
709
710
711 1. Campbell SS, Tobler I. Animal sleep: a review of sleep duration across
712 phylogeny. Neurosci Biobehav Rev. 1984;8(3):269-300. Epub 1984/01/01. PubMed
713 PMID: 6504414.
714 2. Krueger JM, Frank MG, Wisor JP, Roy S. Sleep function: Toward elucidating an
715 enigma. Sleep medicine reviews. 2016;28:46-54. Epub 2015/10/09. doi:
716 10.1016/j.smrv.2015.08.005. PubMed PMID: 26447948; PubMed Central PMCID:
717 PMC4769986.
718 3. Anafi RC, Kayser MS, Raizen DM. Exploring phylogeny to find the function of
719 sleep. Nature reviews Neuroscience. 2019;20(2):109-16. Epub 2018/12/24. doi:
720 10.1038/s41583-018-0098-9. PubMed PMID: 30573905.
721 4. Diekelmann S, Born J. The memory function of sleep. Nature reviews
722 Neuroscience. 2010;11(2):114-26. Epub 2010/01/05. doi: 10.1038/nrn2762. PubMed
723 PMID: 20046194.
724 5. Van Cauter E, Spiegel K, Tasali E, Leproult R. Metabolic consequences of sleep
725 and sleep loss. Sleep Med. 2008;9 Suppl 1:S23-8. Epub 2008/12/17. doi: 10.1016/S1389-
726 9457(08)70013-3. PubMed PMID: 18929315; PubMed Central PMCID:
727 PMCPMC4444051.
728 6. Irwin MR. Why sleep is important for health: a psychoneuroimmunology
729 perspective. Annu Rev Psychol. 2015;66:143-72. Epub 2014/07/26. doi:
730 10.1146/annurev-psych-010213-115205. PubMed PMID: 25061767; PubMed Central
731 PMCID: PMCPMC4961463.
732 7. Hublin C, Partinen M, Koskenvuo M, Kaprio J. Sleep and mortality: a population-
733 based 22-year follow-up study. Sleep. 2007;30(10):1245-53. Epub 2007/11/01. doi:
734 10.1093/sleep/30.10.1245. PubMed PMID: 17969458; PubMed Central PMCID:
735 PMCPMC2266277.
736 8. Saper CB, Fuller PM, Pedersen NP, Lu J, Scammell TE. Sleep state switching.
737 Neuron. 2010;68(6):1023-42. Epub 2010/12/22. doi: 10.1016/j.neuron.2010.11.032.
738 PubMed PMID: 21172606; PubMed Central PMCID: PMC3026325.
739 9. Bringmann H. Sleep-Active Neurons: Conserved Motors of Sleep. Genetics.
740 2018;208(4):1279-89. Epub 2018/04/06. doi: 10.1534/genetics.117.300521. PubMed
741 PMID: 29618588; PubMed Central PMCID: PMC5887131.
742 10. Wu Y, Masurat F, Preis J, Bringmann H. Sleep Counteracts Aging Phenotypes to
743 Survive Starvation-Induced Developmental Arrest in C. elegans. Curr Biol.
744 2018;28(22):3610-24 e8. Epub 2018/11/13. doi: 10.1016/j.cub.2018.10.009. PubMed
745 PMID: 30416057; PubMed Central PMCID: PMCPMC6264389.
746 11. Sinner M, Masurat F, Ewbank J, Pujol N, Bringmann H. Antimicrobial peptides
747 signal need for sleep from peripheral wounds to the nervous system. bioRxiv.
748 2020:2020.07.02.183806. doi: 10.1101/2020.07.02.183806.
749 12. Schmidt MH. The energy allocation function of sleep: a unifying theory of sleep,
750 torpor, and continuous wakefulness. Neurosci Biobehav Rev. 2014;47:122-53. Epub
751 2014/08/15. doi: 10.1016/j.neubiorev.2014.08.001. PubMed PMID: 25117535.

13. Siegel JM. Sleep viewed as a state of adaptive inactivity. Nature reviews Neuroscience. 2009;10(10):747-53. Epub 2009/08/06. doi: 10.1038/nrn2697. PubMed PMID: 19654581.
14. Krause AJ, Simon EB, Mander BA, Greer SM, Saletin JM, Goldstein-Piekarski AN, et al. The sleep-deprived human brain. Nature reviews Neuroscience. 2017;18(7):404-18. Epub 2017/05/19. doi: 10.1038/nrn.2017.55. PubMed PMID: 28515433.
15. Klinzing JG, Niethard N, Born J. Mechanisms of systems memory consolidation during sleep. Nat Neurosci. 2019;22(10):1598-610. Epub 2019/08/28. doi: 10.1038/s41593-019-0467-3. PubMed PMID: 31451802.
16. Turek M, Lewandrowski I, Bringmann H. An AP2 transcription factor is required for a sleep-active neuron to induce sleep-like quiescence in C. elegans. Curr Biol. 2013;23(22):2215-23. Epub 2013/11/05. doi: 10.1016/j.cub.2013.09.028. PubMed PMID: 24184105.
17. Turek M, Besseling J, Spies JP, Konig S, Bringmann H. Sleep-active neuron specification and sleep induction require FLP-11 neuropeptides to systemically induce sleep. eLife. 2016;5. Epub 2016/03/08. doi: 10.7554/eLife.12499. PubMed PMID: 26949257; PubMed Central PMCID: PMC4805538.
18. Nichols ALA, Eichler T, Latham R, Zimmer M. A global brain state underlies C. elegans sleep behavior. Science. 2017;356(6344). Epub 2017/06/24. doi: 10.1126/science.aam6851. PubMed PMID: 28642382.
19. Steuer Costa W, Van der Auwera P, Glock C, Liewald JF, Bach M, Schuler C, et al. A GABAergic and peptidergic sleep neuron as a locomotion stop neuron with compartmentalized Ca2+ dynamics. Nat Commun. 2019;10(1):4095. Epub 2019/09/12. doi: 10.1038/s41467-019-12098-5. PubMed PMID: 31506439.
20. Maluck E, Busack I, Besseling J, Masurat F, Turek M, Busch KE, et al. A wake-active locomotion circuit depolarizes a sleep-active neuron to switch on sleep. PLoS biology. 2020;18(2):e3000361. Epub 2020/02/23. doi: 10.1371/journal.pbio.3000361. PubMed PMID: 32078631.
21. Busack I, Jordan F, Sapir P, Bringmann H. The OptoGenBox - a device for long-term optogenetics in C. elegans. J Neurogenet. 2020:1-9. Epub 2020/06/17. doi: 10.1080/01677063.2020.1776709. PubMed PMID: 32543249.
22. Sinner MP, Masurat F, Ewbank JJ, Pujol N, Bringmann H. Innate Immunity Promotes Sleep through Epidermal Antimicrobial Peptides. Curr Biol. 2021;31(3):564-77 e12. Epub 2020/12/02. doi: 10.1016/j.cub.2020.10.076. PubMed PMID: 33259791.
23. Konietzka J, Fritz M, Spiri S, McWhirter R, Leha A, Palumbos S, et al. Epidermal Growth Factor Signaling Promotes Sleep through a Combined Series and Parallel Neural Circuit. Curr Biol. 2020;30(1):1-16 e3. Epub 2019/12/17. doi: 10.1016/j.cub.2019.10.048. PubMed PMID: 31839447.
24. Gonzales DL, Zhou J, Fan B, Robinson JT. A microfluidic-induced C. elegans sleep state. Nat Commun. 2019;10(1):5035. Epub 2019/11/07. doi: 10.1038/s41467-019-13008-5. PubMed PMID: 31695031.
25. Makino M, Ulzii E, Shirasaki R, Kim J, You YJ. Regulation of Satiety Quiescence by Neuropeptide Signaling in Caenorhabditis elegans. Front Neurosci. 2021;15:678590. Epub 2021/08/03. doi: 10.3389/fnins.2021.678590. PubMed PMID: 34335159; PubMed Central PMCID: PMCPMC8319666.

26. Xu Y, Zhang L, Liu Y, Topalidou I, Hassinan C, Ailion M, et al. Dopamine receptor DOP-1 engages a sleep pathway to modulate swimming in C. elegans. iScience. 2021;24(4):102247. Epub 2021/04/03. doi: 10.1016/j.isci.2021.102247. PubMed PMID: 33796839; PubMed Central PMCID: PMCPMC7995527.
27. Skora S, Mende F, Zimmer M. Energy Scarcity Promotes a Brain-wide Sleep State Modulated by Insulin Signaling in C. elegans. Cell reports. 2018;22(4):953-66. Epub 2018/02/02. doi: 10.1016/j.celrep.2017.12.091. PubMed PMID: 29386137.
28. Kenyon CJ. The genetics of ageing. Nature. 2010;464(7288):504-12. Epub 2010/03/26. doi: 10.1038/nature08980. PubMed PMID: 20336132.
29. Baugh LR, Hu PJ. Starvation Responses Throughout the Caenorhabditis elegans Life Cycle. Genetics. 2020;216(4):837-78. Epub 2020/12/04. doi: 10.1534/genetics.120.303565. PubMed PMID: 33268389; PubMed Central PMCID: PMCPMC7768255.
30. Weber F, Dan Y. Circuit-based interrogation of sleep control. Nature. 2016;538(7623):51-9. Epub 2016/10/07. doi: 10.1038/nature19773. PubMed PMID: 27708309.
31. Bringmann H. Genetic sleep deprivation: using sleep mutants to study sleep functions. EMBO Rep. 2019;20(3). Epub 2019/02/26. doi: 10.15252/embr.201846807. PubMed PMID: 30804011; PubMed Central PMCID: PMCPMC6399599.
32. Ben Soussia I, El Mouridi S, Kang D, Leclercq-Blondel A, Khoubza L, Tardy P, et al. Mutation of a single residue promotes gating of vertebrate and invertebrate two-pore domain potassium channels. Nat Commun. 2019;10(1):787. Epub 2019/02/17. doi: 10.1038/s41467-019-08710-3. PubMed PMID: 30770809; PubMed Central PMCID: PMCPMC6377628.
33. Silva-Garcia CG, Lanjuin A, Heintz C, Dutta S, Clark NM, Mair WB. Single-Copy Knock-In Loci for Defined Gene Expression in Caenorhabditis elegans. G3 (Bethesda). 2019;9(7):2195-8. Epub 2019/05/09. doi: 10.1534/g3.119.400314. PubMed PMID: 31064766; PubMed Central PMCID: PMCPMC6643881.
34. Roux AE, Langhans K, Huynh W, Kenyon C. Reversible Age-Related Phenotypes Induced during Larval Quiescence in C. elegans. Cell Metab. 2016;23(6):1113-26. Epub 2016/06/16. doi: 10.1016/j.cmet.2016.05.024. PubMed PMID: 27304510.
35. Iwanir S, Tramm N, Nagy S, Wright C, Ish D, Biron D. The microarchitecture of C. elegans behavior during lethargus: homeostatic bout dynamics, a typical body posture, and regulation by a central neuron. sleep. 2013;36(3):385-95. Epub 2013/03/02. doi: 10.5665/sleep.2456. PubMed PMID: 23449971; PubMed Central PMCID: PMC3571756.
36. Yemini E, Lin A, Nejatbakhsh A, Varol E, Sun R, Mena GE, et al. NeuroPAL: A Multicolor Atlas for Whole-Brain Neuronal Identification in C. elegans. Cell. 2021;184(1):272-88 e11. Epub 2020/12/31. doi: 10.1016/j.cell.2020.12.012. PubMed PMID: 33378642.
37. Piggott BJ, Liu J, Feng Z, Wescott SA, Xu XZ. The neural circuits and synaptic mechanisms underlying motor initiation in C. elegans. Cell. 2011;147(4):922-33. Epub 2011/11/15. doi: 10.1016/j.cell.2011.08.053. PubMed PMID: 22078887; PubMed Central PMCID: PMC3233480.
38. Li W, Kang L, Piggott BJ, Feng Z, Xu XZ. The neural circuits and sensory channels mediating harsh touch sensation in Caenorhabditis elegans. Nat Commun.

844 2011;2:315. Epub 2011/05/19. doi: 10.1038/ncomms1308. PubMed PMID: 21587232;
845 PubMed Central PMCID: PMC3098610.
846 39. Laurent P, Soltesz Z, Nelson GM, Chen C, Arellano-Carbajal F, Levy E, et al.
847 Decoding a neural circuit controlling global animal state in C. elegans. eLife. 2015;4.
848 Epub 20150311. doi: 10.7554/eLife.04241. PubMed PMID: 25760081; PubMed Central
849 PMCID: PMCPMC4440410.
850 40. Brenner S. The genetics of Caenorhabditis elegans. Genetics. 1974;77(1):71-94.
851 Epub 1974/05/01. PubMed PMID: 4366476.
852 41. Stiernagle T. Maintenance of C. elegans. WormBook. 2006:1-11. Epub
853 2007/12/01. doi: 10.1895/wormbook.1.101.1. PubMed PMID: 18050451.
854 42. Ahringer A. Reverse genetics. WormBook, ed The C elegans Research
855 Community. 2006. doi: doi/10.1895/wormbook.1.47.1.
856 43. Redemann S, Schloissnig S, Ernst S, Pozniakowsky A, Ayloo S, Hyman AA, et
857 al. Codon adaptation-based control of protein expression in C. elegans. Nat Methods.
858 2011;8(3):250-2. Epub 2011/02/01. doi: nmeth.1565 [pii]10.1038/nmeth.1565. PubMed
859 PMID: 21278743.
860 44. Taylor SR, Santpere G, Weinreb A, Barrett A, Reilly MB, Xu C, et al. Molecular
861 topography of an entire nervous system. Cell. 2021. Epub 2021/07/09. doi:
862 10.1016/j.cell.2021.06.023. PubMed PMID: 34237253.
863 45. Turek M, Besseling J, Bringmann H. Agarose Microchambers for Long-term
864 Calcium Imaging of Caenorhabditis elegans. Journal of visualized experiments : JoVE.
865 2015;(100):e52742. Epub 2015/07/02. doi: 10.3791/52742. PubMed PMID: 26132740;
866 PubMed Central PMCID: PMC4544933.
867 46. Bringmann H. Agarose hydrogel microcompartments for imaging sleep- and
868 wake-like behavior and nervous system development in Caenorhabditis elegans larvae. J
869 Neurosci Methods. 2011;201(1):78-88. Epub 2011/08/02. doi: S0165-0270(11)00418-3
870 [pii]10.1016/j.jneumeth.2011.07.013. PubMed PMID: 21801751.
871 47. Nagy S, Raizen DM, Biron D. Measurements of behavioral quiescence in
872 Caenorhabditis elegans. Methods. 2014. Epub 2014/03/20. doi:
873 10.1016/j.ymeth.2014.03.009. PubMed PMID: 24642199.
874

875